Volume 9 | Number 21 | 7 November 2025

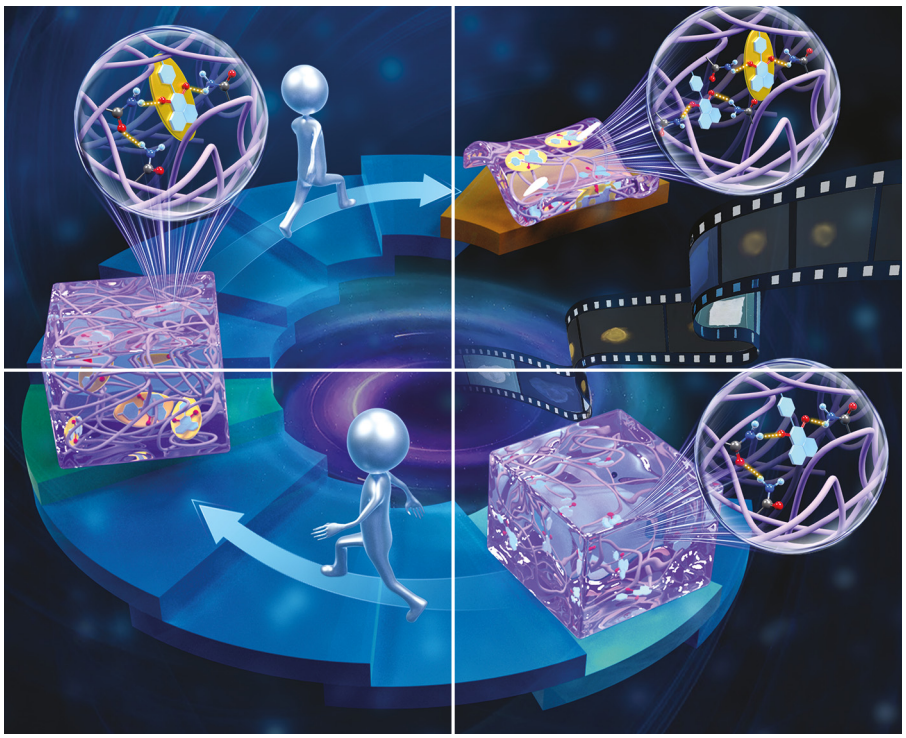

MATERIALS CHEMISTRY

FRONTIERS

CCS 中国化学会 CHINESE CHEMICAL SOCIETY

ICCAS 1956

ROYAL SOCIETY OF CHEMISTRY

rsc.li/frontiers-materials

MATERIALS CHEMISTRY FRONTIERS

RESEARCH ARTICLE

View Article Online
View Journal | View Issue

Cite this: *Mater. Chem. Front.*, 2025, **9**, 3139

Constructing highly efficient dual-confinement phosphorescence supramolecular naphthalimide pyridinium networks *via* eco-friendly post-polymerization assembly

Qi Song,†[a] Xianfeng Meng,†[a] Xue Bai,[a] Yongbin Sun,[a] Yanqing Ge[a] and Xian-Yin Dai*[ab]

Developing supramolecular network materials with controllable phosphorescence behavior constitutes a highly active research frontier. Herein, the preparation of a high-efficiency room-temperature phosphorescence (RTP) supramolecular polymer network (SPN) *via* the post-polymerization assembly strategy is reported, through sequential polymerization of naphthalimide pyridinium derivatives and spontaneous aqueous self-assembly with exfoliated LAPONITE® (LP) nanosheets. Initially, thermally initiated copolymerization of cationic naphthalimide pyridinium derivatives with acrylamide produces transparent swollen hydrogels by solvent replacement, exhibiting emergent RTP with a lifetime of 29.1 μs governed by hydrogen-bonding confinement. Subsequent electrostatic integration of negatively charged LP nanosheets into hydrogels can tightly anchor cationic naphthalimide pyridinium moieties, thus extending the phosphorescence lifetime to 923 μs by further suppressing the non-radiative transition of triplet excitons. Crucially, dual spatial confinement—from both interwoven hydrogen-bonding networks coupled with rigid LP nanosheet architectures—synergistically elevates the RTP lifetime to 316.0 ms with an excellent phosphorescence quantum yield of up to 67.5% in free-standing dehydrated SPN films, representing a 340-fold improvement over the pristine hydrogels by circumventing aqueous-mediated quenching pathways. This hierarchical confinement strategy enables dynamic information processing and penetrated bioimaging applications, offering a versatile platform for designing RTP materials with tailorable photophysics.

Received 1st August 2025,
Accepted 21st August 2025

DOI: 10.1039/d5qm00579e

rsc.li/frontiers-materials

Introduction

Supramolecular polymer networks (SPNs) mediated by reversible non-covalent interactions represent an attractive frontier in modern materials science and biomedical research due to their unique self-assembly capabilities and stimuli-responsive behaviors.[1–5] In particular, the elegant incorporation of functional luminophores into SPNs can endow the resultant supramolecular systems with fascinating photoluminescence properties, which hold tremendous promise in critical applications including controlled drug release,[6,7] chemical sensors,[8–10] light-harvesting systems,[11–13] adhesives,[14,15] optoelectronic devices,[16,17] information encoding,[18–20] adsorptive separation materials,[21,22] and so on. Synthetic macrocycles have played important roles in the construction of fluorescent SPNs with the aid of host–guest interactions of different recognition pairs, not only promoting the formation of dense polymer networks through the tight encapsulation of guest fluorophores in their intrinsic cavities,[23–25] but also inducing or improving the photoluminescence performance such as high quantum yields of the guest molecules through spatial confinement effects.[26–28] For example, Yang and co-workers reported highly emissive SPNs with an extremely high fluorescence quantum yield of up to 98.22% by utilizing the combination of pillar[5]arene-functionalized copolymers and tetraphenylethylene-based tetratopic guests *via* supramolecular host–guest interactions.[29] Yan and co-workers also prepared clusterization-triggered emissive SPNs through pillar[5]arene-grafted poly(methyl methacrylate) and merocyanine-containing guest polymers whose fluorescence could be reversibly regulated by adjusting pH conditions.[30] Liu *et al.* reported supramolecular hydrogel networks with multicolor emissions especially white light based on the orthogonal supramolecular self-sorting recognitions of adamantyl and sulfonatocalix[4]arene moieties.[31] Conclusively, these

[a] *School of Chemistry and Pharmaceutical Engineering, Shandong First Medical University & Shandong Academy of Medical Sciences, Taian, 271016, China. E-mail: daixianyin@sdfmu.edu.cn*
[b] *State Key Laboratory of Molecular Engineering of Polymers, Fudan University, Shanghai 200438, China*
† Qi Song and Xianfeng Meng contributed equally to this work.

aforementioned studies have offered unique viewpoints for the creation of new supramolecular matter with favorable fluorescence performance based on SPNs.

Different from conventional fluorescence from excited singlet excitons, organic room temperature phosphorescence (RTP) originates from the slow radiative transition of triplet excitons and therefore has the unique characteristics of longer lifetime and larger Stokes shift,[32–34] and is widely utilized in anticounterfeiting,[35–38] bioimaging,[39–41] information encryption,[42–45] and optoelectronic display applications.[46–49] Consequently, the exploration of SPNs with RTP behavior has become an active research area, which is of great practical significance for further expanding their photonic applications. Departing from conventional RTP systems reliant on physically doped luminophores prone to aggregation-induced quenching and spectral shifts, the covalently engineered SPNs achieve molecular-level precision *via in situ* integration of luminophores during polymerization.[50–52] This synthetic strategy eliminates concentration-dependent optical degradation through spatial control of chromophore distribution.[53–55] Moreover, the hierarchically rigid architecture further imposes three-dimensional confinement by combining covalent immobilization of phosphors in optimized geometries, hydrogen-bond-reinforced chain packing, and oxygen-blocking nanodomains, collectively suppressing nonradiative relaxation pathways.[56–58] For instance, Ma and co-workers prepared self-healable near-infrared RTP emitting gels from the polymerization of ureidopyrimidone moieties and the iodine substituted borondipyrromethene.[59] Yang *et al.* reported a flexible cross-linked polymer network from the polycondensation reaction between multifunctional aromatic amine, a crosslinker and a curing agent, which showed high phosphorescence quantum efficiency as well as thermo-responsive phosphorescence behavior.[60] Despite significant progress in the construction of cross-linked RTP networks being achieved, it is still highly desirable to seek out a facile and universal method to realize efficient phosphorescent SPNs in both hydrogel and solid states.

In this study, we report a class of high-efficiency phosphorescence naphthalimide pyridinium-based SPNs *via* a post-polymerization assembly strategy in aqueous solution (Fig. 1). Firstly, two different monoalkene-functionalized naphthalimide-pyridinium derivatives were designed for the one-pot thermally initiated free-radical copolymerization with acrylamide (AAm), which can form transparent hydrogels after solvent exchange with emergent RTP (τ = 29.1 μs) by virtue of the hydrogen-bonding confinement. Moreover, benefiting from the strong electrostatic interactions, negatively charged LAPONITE® (LP) nanosheets were further introduced to anchor a cationic naphthalimide-pyridinium moiety thus endowing the hydrogels with an improved RTP lifetime of 923 μs. Owing to the cooperative spatial confinement combining persistent hydrogen-bond networks with rigid LP nanosheet architectures, the RTP lifetime was ultimately improved to 316.0 ms in freestanding solid SPN films, which were successfully applied in afterglow patterns for information encryption and penetrated bioimaging. This study presents a novel supramolecular paradigm to create RTP SPN materials through rational hierarchical confinement engineering.

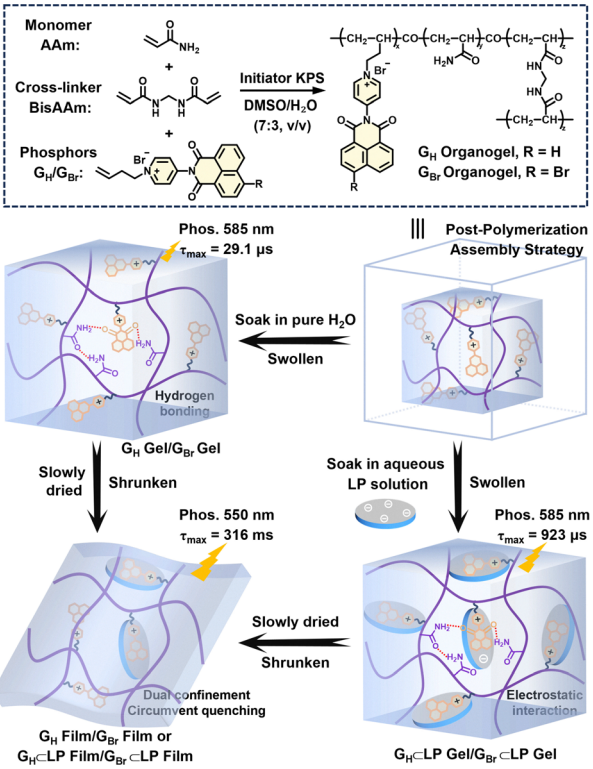

Fig. 1 Schematic depiction of the synthesis of phosphorescence SPN films based on naphthalimide pyridinium derivatives through a post-polymerization aqueous assembly strategy.

Results and discussion

Two distinct heavy-atom-free, bromo-substituted *N*-pyridyl-1,8-naphthalimide derivatives were designed and synthesized (abbreviated as G_H and G_{Br}, respectively). In these compounds, the nitrogen atom position in the pyridine moiety was functionalized with vinyl aliphatic chains. The synthesis of the corresponding naphthalimide pyridinium derivatives G_H and G_{Br} is systematically outlined in Scheme S1, with their molecular structures unequivocally confirmed by comprehensive spectroscopic characterization, including ^{1}H NMR spectroscopy, ^{13}C NMR spectroscopy, and HR-MS (Fig. S1–S6). It was expected that the monoalkene-functionalized, positively charged pyridinium salt could participate in radical copolymerization with acrylamide (AAm), followed by electrostatic assembly with negatively charged LP nanosheets. It has been reported that the bromine atoms in the *N*-pyridyl-1,8-naphthalimide derivative promoted efficient intersystem crossing (ISC) to the triplet state *via* the heavy-atom effect, relative to heavy-atom-free counterpart.[61–63] To investigate the co-assembly process of G_{Br} with LP in aqueous solution, UV-Vis spectroscopy was first performed. As shown in Fig. 2a, the UV-Vis absorption spectrum of G_{Br} initially exhibited a maximum peak at 350 nm. Upon the gradual addition of LP, this peak red-shifted to 354 nm due to the rigid confinement effect of nanosheets, and the absorption intensity gradually increased, reaching saturation at an LP concentration of 6.0 mg mL^{-1} (Fig. S7). The photoluminescence (PL) spectrum of free G_{Br} displayed a

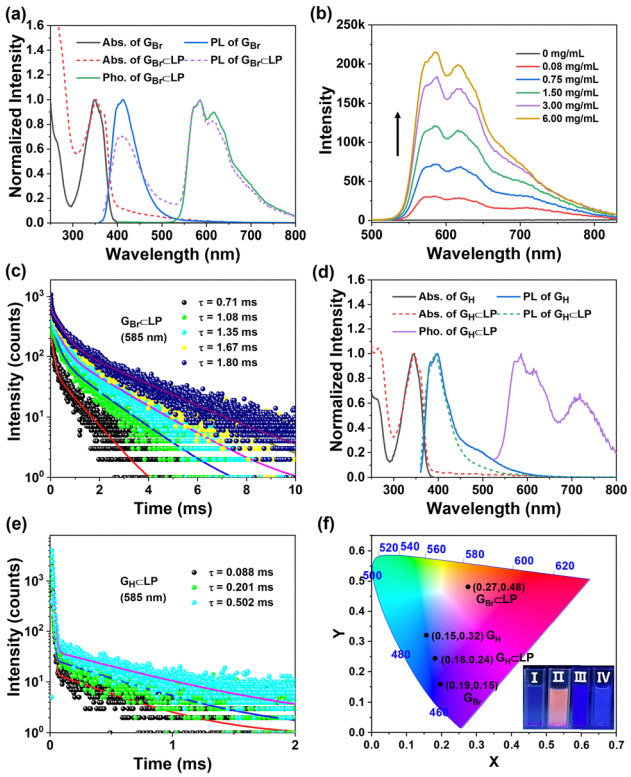

Fig. 2 (a) Normalized absorption spectra of G_{Br} and G_{Br}⊂LP, prompt photoluminescence spectra of G_{Br} and G_{Br}⊂LP, and the gated emission spectrum (delay 100 μs) of G_{Br}⊂LP in aqueous solution at 298 K ($[G_{Br}]$ = 1.0×10^{-5} M, [LP] = 6.0 mg mL^{-1}, and λ_{ex} = 350 nm). (b) Phosphorescence emission spectra (delay 100 μs) of G_{Br} in aqueous solution upon the addition of 0, 0.08, 0.75, 1.50, 3.00, and 6.00 mg mL^{-1} LP at 298 K ($[G_{Br}]$ = 1.0×10^{-5} M, λ_{ex} = 350 nm). (c) Time-resolved photoluminescence decay spectra of G_{Br} at 585 nm upon the stepwise addition of 0.08, 0.75, 1.50, 3.00, and 6.00 mg mL^{-1} LP in aqueous solution at 298 K, respectively. (d) Normalized absorption spectra of G_H and G_H⊂LP, prompt photoluminescence spectra of G_H and G_H⊂LP, and the gated emission spectrum (delay 100 μs) of G_H⊂LP in aqueous solution at 298 K ($[G_H]$ = 1.0×10^{-5} M, [LP] = 1.50 mg mL^{-1}, and λ_{ex} = 345 nm). (e) Time-resolved photoluminescence decay spectra of G_H at 585 nm upon the stepwise addition of 0.08, 0.75, and 1.50 mg mL^{-1} LP in aqueous solution at 298 K, respectively. (f) The CIE 1976 chromaticity diagram of G_{Br}, G_{Br}⊂LP, G_H, and G_H⊂LP in aqueous solution. Inset: the corresponding photographic images of (I) G_{Br} and (II) G_{Br}⊂LP (III) G_H and (IV) G_H⊂LP upon illumination with UV light.

broad emission peak at 411 nm with a lifetime of 0.55 ns which belonged to fluorescence emission (Fig. S9a). After LP addition, the emission peak blue-shifted to 408 nm and the lifetime increased to 0.92 ns (Fig. S8 and S9b), while an emergent emission peak was observed at 585 nm/615 nm. Time-gated spectroscopy also revealed new emission bands at 585 nm and 615 nm upon LP addition, with emission intensities plateauing at an LP concentration of 6.0 mg mL^{-1} (Fig. 2a, b and Fig. S10). As the LP concentration increased, the lifetimes at 585 nm and 615 nm increased from 0.71 ms/0.71 ms to 1.84 ms/1.91 ms, respectively (Fig. 2c and Fig. S11). These results indicated that the new peak at 585 nm/615 nm originated from aqueous phosphorescence emission. Consistent with the PL spectral changes, a distinct luminescence color change was observed under UV light, with the solution color shifting from initial blue to reddish upon assembly with LP (Fig. 2f, inset). The CIE 1976 chromaticity diagram confirmed this color shift, showing coordinate movement from (0.19, 0.15) to (0.27, 0.48) (Fig. 2f). The emergence of phosphorescence emission could be attributed to the co-assembly mediated by electrostatic interactions between positively charged G_{Br} and the complementary negatively charged LP nanosheets. The confinement effect of the rigid LP matrix could tightly rigidify the chromophores which was beneficial for the restriction of the phosphor motion and reduction of the non-radiative decay pathways thereby inducing phosphorescence. The synergy between the intramolecular heavy-atom effect and the LP-based rigidity confinement enabled effective RTP emission in aqueous solution.

Unlike the G_{Br}-substituted analogue, the co-assembly of G_H with LP produced different photoluminescence behavior in aqueous solution due to the lack of an intramolecular heavy atom for the G_H derivative. As depicted in Fig. 2d, free G_H exhibited a primary absorption peak at 345 nm in its UV-Vis spectrum, which almost remained unaltered upon LP addition (Fig. S12). The PL spectrum of free G_H showed a broad fluorescence emission peak at 400 nm with a lifetime of 2.26 ns. Following LP incorporation, this emission peak shifted to a shorter wavelength at 393 nm, accompanied by a slight lifetime reduction to 2.06 ns (Fig. S13 and S14). In contrast to the single emission band at 393 nm observed in the steady-state PL spectrum of the G_H⊂LP complex, time-gated spectroscopy (100 μs delay) uncovered additional emission bands at 585 nm and 720 nm. Their intensities reached saturation at an LP concentration of 1.50 mg mL^{-1} (Fig. S15). The lifetimes at 585 nm/720 nm of G_H⊂LP assembly increased from 0.088 ms/2.67 μs to 0.502 ms/4.25 μs, respectively (Fig. 2e and Fig. S16). However, these lifetimes were significantly shorter than those observed for G_{Br}⊂LP assembly, which likely attributable to lower ISC efficiency in G_H, stemming from the absence of bromine atoms in its molecular structure. Therefore, the G_H solution still maintained a blue emission color under UV irradiation after assembly with LP, with the CIE 1976 chromaticity coordinates showing a subtle shift from (0.15, 0.32) to (0.18, 0.24) (Fig. 2f, inset). Although the supramolecular assembly between G_H and LP paralleled that of G_{Br}, with both systems relying on electrostatic interactions combined with LP-induced rigid confinement to activate aqueous phosphorescence. However, the absence of bromine atoms in G_H decreased its ISC efficiency relative to G_{Br}, which led to the insufficient RTP emission in aqueous solution compared with G_H under the same ambient conditions.

After fully characterizing the assembly-induced aqueous RTP behaviors of cationic G_{Br}/G_H and LP, these two naphthalimide pyridinium derivatives were further employed as functional monomers to copolymerize with acrylamide (AAm) and *N*,*N*′-methylenebisacrylamide (bisAAm) *via* free radical polymerization, in anticipation of constructing three-dimensional phosphorescent supramolecular hydrogel networks. The reaction was conducted in a DMSO/H_2O (7 : 3, v/v) mixed solvent system using potassium persulfate as a thermal initiator at 70 °C. After polymerization, the homogeneous solution yielded

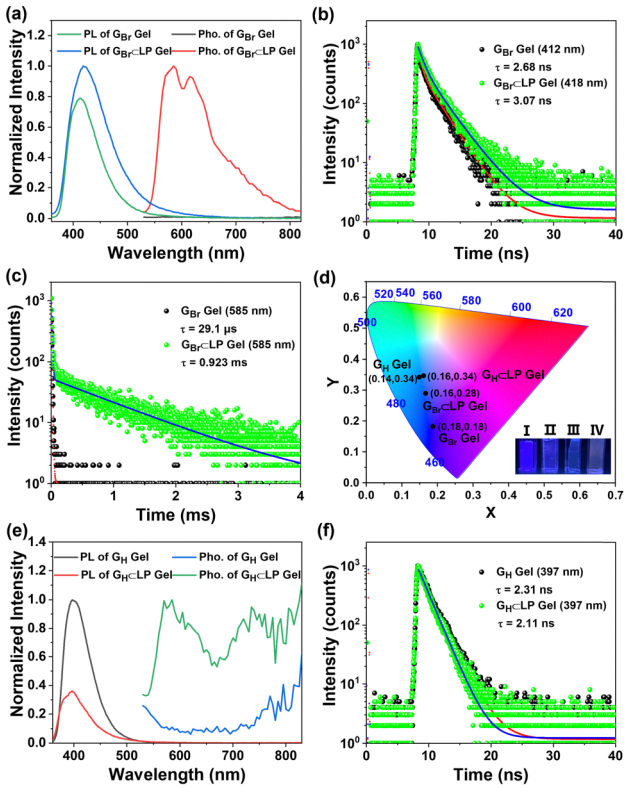

Fig. 3 (a) Normalized prompt photoluminescence spectra of the G_{Br} gel and G_{Br}⊂LP gel, and the gated emission spectrum (delay 100 μs) of the G_{Br} gel and G_{Br}⊂LP gel at 298 K (λ_{ex} = 350 nm). Time-resolved photoluminescence decay spectra of the G_{Br} gel at (b) 412 nm (c) 585 nm and the G_{Br}⊂LP gel at (b) 418 nm and (c) 585 nm at 298 K. (d) The CIE 1976 chromaticity diagram of the G_{Br} gel, G_{Br}⊂LP gel, G_H gel, and G_H⊂LP gel. Inset: The corresponding photographic images of the (I) G_H gel and (II) G_H⊂LP gel and (III) G_{Br} gel and (IV) G_{Br}⊂LP gel upon illumination with UV light. (e) Normalized prompt photoluminescence spectra of the G_H gel and G_H⊂LP gel, and gated emission spectrum (delay 100 μs) of the G_H gel and G_H⊂LP gel at 298 K (λ_{ex} = 345 nm). (f) Time-resolved photoluminescence decay spectra of the G_H gel at 397 nm and G_H⊂LP gel at 397 nm at 298 K.

a uniform gel, which was purified by washing with DMSO and water several times to remove unreacted monomers. Subsequently, the resulting gels were separately immersed in an excess amount of pure aqueous solution or treated with an LP aqueous solution for 48 h to reach equilibrium, which finally produced the G_{Br}/G_H gel and G_{Br}/G_H⊂LP gel by a solvent replacement method, respectively. To screen for the optimal concentration of the aqueous LP solution, a series of PL performance tests were conducted on the resulting swollen hydrogels. Steady-state PL measurements showed an emission peak at 412 nm for the G_{Br} gel (Fig. 3a). In contrast, the G_{Br}⊂LP gel exhibited a red-shifted emission peak at 418 nm (Fig. S17). Notably, significant differences were observed in their time-gated emission spectra (delay time = 100 μs). The G_{Br} gel displayed weak dual emission peaks at 585 nm and 620 nm, whereas the G_{Br}⊂LP gel showed strong dual emissions (Fig. S18). Further time-resolved PL decay analysis confirmed that the 412 nm emission in the G_{Br} gel corresponded to short-lived fluorescence with a lifetime of 2.68 ns. The emissions at 585 nm and 620 nm were assigned to emergent phosphorescence, exhibiting lifetimes of 29.1 μs and 66.0 μs, respectively. This newly appeared phosphorescence stemmed from the effective spatial hydrogen-bonding confinement effect within the rigid and compact 3D supramolecular polymeric networks. Similarly, the G_{Br}⊂LP gel also exhibited nanosecond-scale fluorescence (τ = 3.07 ns) at 418 nm, while its phosphorescence lifetimes at 585 nm and 620 nm were significantly prolonged to 0.923 ms and 0.892 ms, respectively (Fig. 3b, c and Fig. S19). These observations indicate that negatively charged LP nanosheets successfully assembled into the cationic polymer networks *via* electrostatic interactions, thereby enhancing the phosphorescence performance of the G_{Br}⊂LP gel. Furthermore, the CIE 1976 chromaticity diagram revealed that the color coordinates of the G_{Br} gel (0.18, 0.18) and G_{Br}⊂LP gel (0.16, 0.28) are closely positioned, suggesting the similar emission colors (Fig. 3d).

For the G_H-based hydrogel system, both the G_H gel and the G_H⊂LP gel exhibited a steady-state PL emission peak at 397 nm (Fig. 3e). However, their delayed spectra showed distinct differences; no delayed emission was observed for the G_H gel, while the G_H⊂LP gel displayed a weak emission peak at 585 nm (Fig. 3e and Fig. S20, S21). Lifetime measurements revealed that the 397 nm emissions for both the G_H gel and the G_H⊂LP gel were short-lived fluorescence, with lifetimes of 2.31 ns and 2.11 ns, respectively (Fig. 3f). Nevertheless, the G_H⊂LP gel exhibited microsecond-scale phosphorescence (τ = 23.1 μs) at 585 nm, confirming its long-lived luminescence characteristics (Fig. S22). The CIE chromaticity diagram further demonstrated nearly overlapping color coordinates for the G_H gel (0.14, 0.34) and G_H⊂LP gel (0.16, 0.34), indicating highly consistent emission colors (Fig. 3d). The G_{Br}⊂LP gel and G_H⊂LP gel exhibited significantly weaker emission intensities and phosphorescence lifetimes compared to the G_{Br}⊂LP and G_H⊂LP assemblies in aqueous solution. This attenuation is presumably attributed to the insufficient adsorption of LP nanosheets within the hydrogel matrix, a phenomenon primarily arising from the spatial constraints imposed by the hydrogel's intricate three-dimensional network. These structural limitations hinder the full and effective assembly between the cationic naphthalimide-pyridinium functional moieties distributed throughout the polymer network and the negatively charged surfaces of LP nanosheets, thereby impeding the formation of robust electrostatic and interfacial interactions that are critical for stabilizing the composite structure. At an LP aqueous concentration of 5.0 mg mL^{-1}, the swollen hydrogel exhibited maximal phosphorescence performance; thus, this concentration was consequently designated for above and subsequent experiments. Additionally, in contrast to the G_{Br} gel and G_H gel, the obvious enhancement in phosphorescence performance particularly the prolonged lifetimes observed in the G_{Br}⊂LP gel and G_H⊂LP gel, suggesting that the supramolecular architecture formed between the LP nanosheets and the polymer network created a relatively rigid microenvironment. This microenvironment effectively suppressed molecular vibrations and non-radiative relaxation processes, stabilizing the triplet excited state and thereby significantly improving the phosphorescence

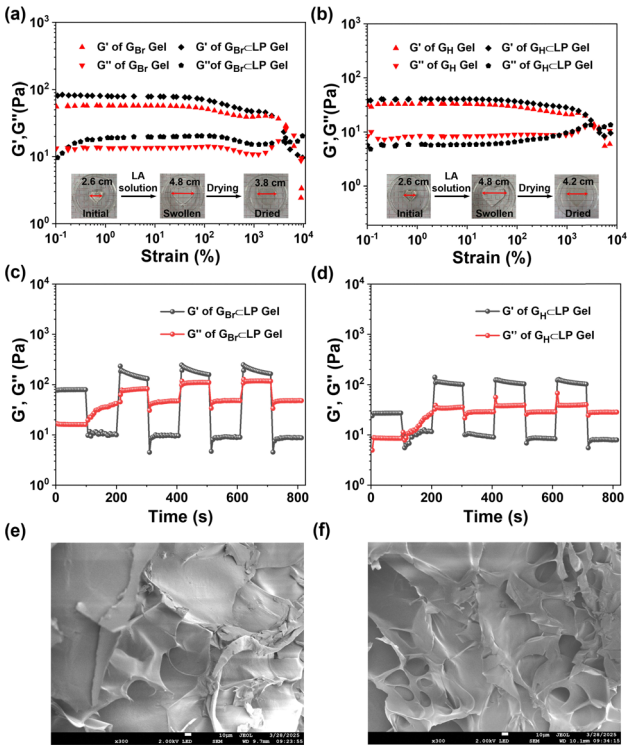

Fig. 4 (a) Dynamic strain sweep curves at γ = 0.1–10 000% with fixed ω = 6.28 rad s^{-1} at 298 K (red, G_{Br} gel; black, G_{Br}⊂LP gel). Inset: Photographs of the initially prepared gel, swollen G_{Br}⊂LP gel, and dried G_{Br}⊂LP gel, respectively. (b) Dynamic strain sweep curves at γ = 0.1–10 000% with fixed ω = 6.28 rad s^{-1} at 298 K (red, G_H gel; black, G_H⊂LP gel). Inset: Photographs of the initially prepared gel, swollen G_H⊂LP gel, and dried G_H⊂LP gel, respectively. (c) Continuous step strain curves of the G_{Br}⊂LP gel at γ = 1 and 100% with fixed ω = 6.28 rad s^{-1} at 298 K. (d) Continuous step strain curves of the G_H⊂LP gel at γ = 1 and 100% with fixed ω = 6.28 rad s^{-1} at 298 K. Scanning electron microscopy (SEM) images of the lyophilized (e) G_{Br}⊂LP gel and (f) G_H⊂LP gel.

properties of the hydrogels. This finding provides important insights for designing novel long-lived luminescent materials through an eco-friendly post-polymerization assembly strategy.

Subsequently, rheological characterization was conducted to assess the mechanical properties of these supramolecular swollen hydrogels. Photographs of completely shrunken and fully swollen hydrogels are presented in Fig. 4a, b and Fig. S23. All of the resulting hydrogels were transparent and colorless, where the prepared hydrogels presented high transparency under ambient conditions, and the transmittance of hydrogels in the visible wavelength almost reached 90% (Fig. S24). Compared with G_{Br}/G_H gel, the swelling ratio of the G_{Br}/G_H⊂LP gel was increased from 3.23 and 3.51 to 4.12 and 4.25, respectively, when they were fully swollen in water. The better swelling properties of the G_{Br}/G_H⊂LP gel were attributed to the presence of LP nanosheets which generated strong electrostatic repulsion between polymer chains due to their negatively charged feature. Rheology experiments illustrated that the fully swollen hydrogel had certain mechanical strength. The dynamic strain sweep tests (fixed angular frequency of 6.28 rad s^{-1}) showed that all hydrogels maintained a constant storage modulus (G') and a loss modulus (G'') within the strain range of 0.1–3000%, confirming the structural stability of the physically crosslinked supramolecular network. When the strain exceeded the critical value (G_{Br} gel, γ = 4418.3%; G_{Br}⊂LP gel, γ = 4359.4%; G_H gel, γ = 3456.1%; G_H⊂LP gel, γ = 3002.5%) the decline rate of G' was significantly faster than that of G'', indicative of the network collapse (Fig. 4a and b). Notably, the mechanical properties of the LP-integrated G_{Br}⊂LP gel and G_H⊂LP were enhanced, with both G' and G'' being higher than those of the free G_{Br} gel. The dynamic frequency sweep curves showed that G' remained larger than G'' within the range of tested angular frequency and did not change obviously with the fixed 1% strain (Fig. S25), implying the good stability of the hydrogels towards frequency oscillation. Step-strain tests further verified the excellent structural reversible recovery properties of the hydrogels (Fig. 4c, d and Fig. S26, S27), which showed the rapid self-healing capability after damage and this process could be repeated for several times. Scanning electron microscopy (SEM) images showed that the lyophilized G_{Br} gel and G_H gel exhibited typical three-dimensional porous network structures (Fig. S28 and S29), while a number of lamellar sheets with poriferous structures were observed for G_{Br}⊂LP gel and G_H⊂LP gel, suggesting the retention of the sheet-like structure of LP in the hydrogel (Fig. 4e and f). These results jointly confirmed the successful integration of negatively charged LP nanosheets into cationic polymer hydrogel networks through electrostatic interactions, which resulted in the better swelling properties and improved mechanical strength for the G_{Br}⊂LP gel and G_H⊂LP gel.

Although LP-integrated G_{Br}⊂LP and G_H⊂LP hydrogels exhibited improved RTP compared to G_{Br} and G_H hydrogels, attributable to the synergistic dual hydrogen-bond crosslinking network and non-covalent assembly confinements, they remained susceptible to quenching of triplet excitons by high concentrations of water molecules. This further led us to investigate whether slow drying hydrogels to form homogeneous films could enhance their intrinsic phosphorescence performance. The free-standing films were conveniently obtained by drying the hydrogels to fully remove any moisture. SEM images revealed a flat and smooth film interface for all films, signifying the formation of a highly uniform and compact structure (Fig. 5a and b, inset and Fig. S30 and S31). These observations prompted us to perform an in-depth investigation into their luminescence properties. Both the G_{Br} film and the G_{Br}⊂LP film showed two distinct emission bands at about 398 nm and 575 nm in steady-state PL spectra, but the PL intensity of the G_{Br}⊂LP film was significantly enhanced in comparison to the G_{Br} film (Fig. 5a, b and Fig. S32). Time-resolved PL decay analyses further confirmed that the lifetimes at 398 nm for both the G_{Br} film and the G_{Br}⊂LP film were 1.82 ns and 2.74 ns at a nanosecond-scale, respectively (Fig. 5f and Fig. S33), which suggested that the emissions at 398 nm were attributed to short-lived fluorescence. Time-gated emission spectra (delay time = 100 μs) unveiled differences in long-lived luminescence: the G_{Br} film exhibited dual phosphorescence peaks at 575 nm and 610 nm, whereas the G_{Br}⊂LP film, despite similar peak positions, showed significantly prolonged

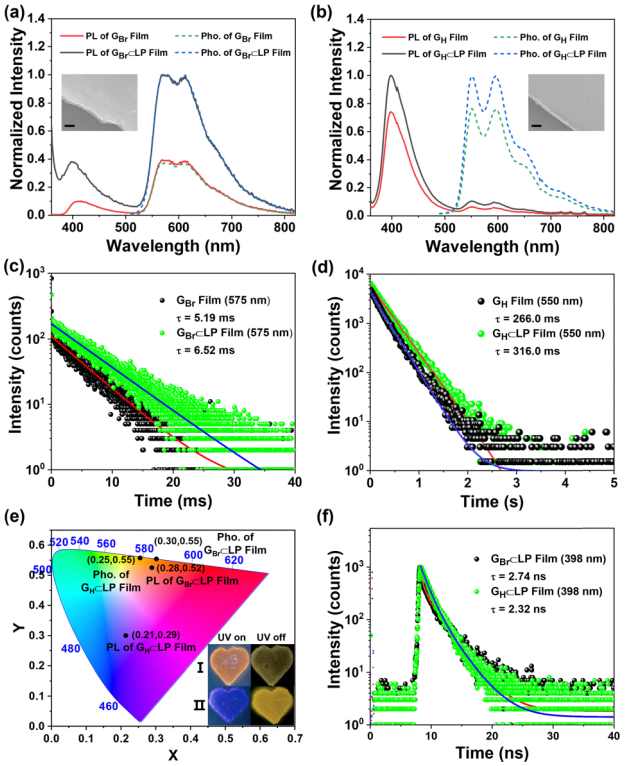

Fig. 5 (a) Normalized prompt photoluminescence spectra of the G_{Br} film and G_{Br}⊂LP film, and the gated emission spectrum (delay 100 μs) of the G_{Br} film and G_{Br}⊂LP film at 298 K (λ_{ex} = 350 nm). Inset: SEM image of the G_{Br}⊂LP film. The scale bar is 30 μm. (b) Normalized prompt photoluminescence spectra of the G_H film and G_H⊂LP film, and the gated emission spectrum (delay 100 μs) of the G_H film and G_H⊂LP film at 298 K (λ_{ex} = 345 nm). Inset: SEM image of the G_H⊂LP film. The scale bar is 30 μm. (c)Time-resolved photoluminescence decay spectra of the G_{Br} film and G_{Br}⊂LP film at 575 nm at 298 K. (d) Time-resolved photoluminescence decay spectra of the G_H film and G_H⊂LP film at 550 nm at 298 K. (e) The CIE 1976 chromaticity diagram of the G_{Br}⊂LP film and G_H⊂LP film. Inset: Photographs of the luminescence of the (I) G_{Br}⊂LP film and (II) G_H⊂LP film before and after switching off UV light. (f) Time-resolved photoluminescence decay spectra of the G_{Br}⊂LP film and G_H⊂LP film at 398 nm at 298 K.

phosphorescence lifetimes (increasing from 5.19/5.26 ms to 6.52/6.38 ms) and improved phosphorescence intensities (increasing 2.5 times) (Fig. 5c and Fig. S34, S35). It was noted that the G_{Br}⊂LP film presented an extraordinary phosphorescence quantum yield of up to 67.5% under ambient conditions (Fig. S36). CIE 1976 chromaticity coordinates showed that the PL coordinates of the G_{Br} film were (0.29, 0.53), with phosphorescence coordinates of (0.30, 0.55), appearing orange-red color under UV light and exhibiting a slight shift in afterglow upon UV cutoff (Fig. S37). In contrast, the G_{Br}⊂LP film had PL coordinates of (0.28, 0.52) and phosphorescence coordinates of (0.30, 0.55), emitting orange-red light under UV irradiation and transitioning to yellow afterglow upon UV removal (Fig. 5e). Therefore, it can be inferred that, LP as a layered nanoclay possessing hydroxyl-rich surfaces, could serve as hydrogen-bonding sites after dehydration, mediating extensive networks between organic phosphorescent molecules and polyacrylamide chains, thus suppressing nonradiative decay and improving their phosphorescence performance.

Analogously, both the G_H film and the G_H⊂LP film displayed fluorescence peaks at 398 nm with nanosecond-scale lifetimes (τ = 2.40/2.32 ns) (Fig. 5f and Fig. S33), whereas their delayed spectra featured phosphorescence peaks at 550 nm and 596 nm (Fig. 5b and Fig. S38–S39). Notably, the phosphorescence lifetimes of the G_H⊂LP film (316.0 ms/313.8 ms) were significantly prolonged compared to those of the G_H film (266.0/258.8 ms) (Fig. 5d and Fig. S40). The phosphorescence quantum yield of the G_H⊂LP film was determined to be 18.0% under ambient conditions (Fig. S41). In terms of CIE coordinates, the G_H film had PL coordinates of (0.21, 0.28) and phosphorescence coordinates of (0.25, 0.55) (Fig. S37), appearing blue under UV excitation and transitioning to yellow afterglow after UV removal; the G_H⊂LP film showed a similar trend, with PL coordinates of (0.21, 0.29) and phosphorescence coordinates of (0.25, 0.55) (Fig. 5e). These results demonstrated that the enhanced structural density and rigidity by forming free-standing films as well as the introduction of LP nanosheets could effectively suppress non-radiative transitions and mitigated quenching induced by the surrounding environment, therefore resulting in the

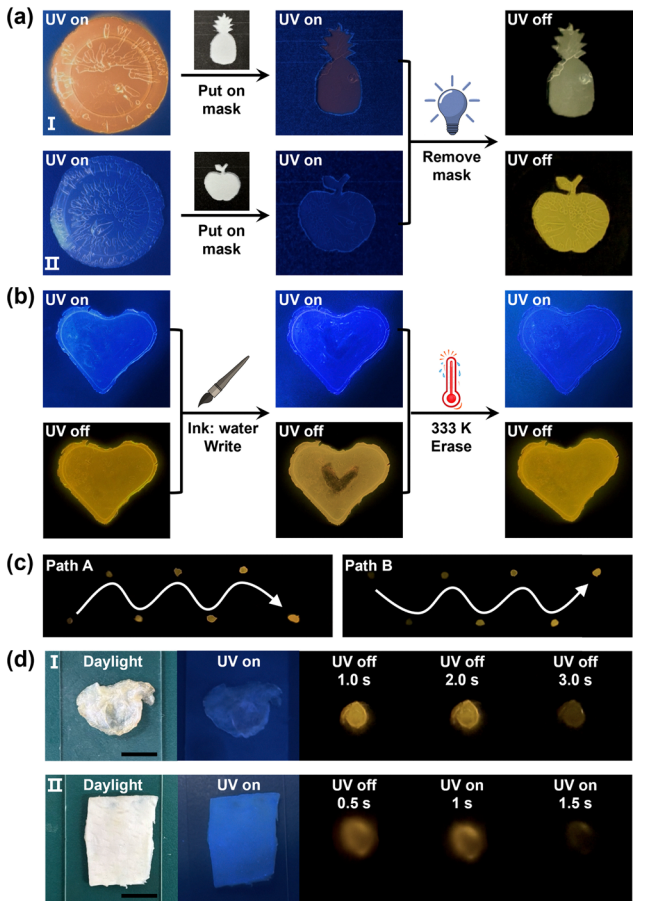

Fig. 6 (a) Afterglow patterns prepared using the (I) G_{Br}⊂LP film and (II) G_H⊂LP film. (b) Schematic illustration of the information data processing based on the G_H⊂LP film. (c) Afterglow display of different UV moving paths (λ_{ex} = 365 nm). (d) The photographs captured behind a piece of the skin from a (I) chicken (thickness: 0.8 mm) or (II) pork (thickness: 1.2 mm) (scale bar = 1 cm).

stabilization of triplet excitons for efficient RTP emission *via* synergistically covalent and non-covalent confinement effects.

Given the excellent RTP properties of SPN films, their applications in information data processing and bioimaging of penetrating a piece of skin were further investigated. Specifically, irradiation of a G_{Br}⊂LP film through a pineapple-shaped photomask with 365 nm UV light produced a corresponding pineapple pattern exhibiting pale yellow afterglow upon UV removal, while irradiation of a G_H⊂LP film through an apple-shaped photomask yielded an apple pattern with yellow afterglow (Fig. 6a). This enabled on-demand customization of phosphorescent patterns through varied photomask designs. Furthermore, leveraging the reversible water-quenching characteristic of the phosphorescence, water served as "ink" for rewritable encryption; writing the letter "V" on a G_H⊂LP film created a quenched region that contrasted sharply with the surrounding phosphorescence, with the information erasable and afterglow recoverable *via* thermal treatment (Fig. 6b). However, the letter "V" on the G_H⊂LP film was very difficult to identify under UV light. The material also enabled dynamic light-path tracking: scanning with a mobile 365 nm UV source resulted in time-dependent afterglow intensity, where previously irradiated points showed weaker emission and later points exhibited stronger emission, clearly visualizing the light path A and B (Fig. 6c). In addition, both chicken and pork skin exhibited blue autofluorescence under UV light; however, upon lamp extinction, a persistent orange afterglow from the G_H⊂LP film can be clearly seen through the tissue, demonstrating its effectiveness in eliminating tissue autofluorescence and background fluorescence interference (Fig. 6d). These functionalities collectively highlight the significant potential of SPN films in rewritable information storage, dynamic optical recording, and deep-tissue penetrated bioimaging.

Conclusions

In conclusion, we have constructed an efficient dual-confinement room-temperature phosphorescence (RTP) supramolecular polymer network (SPN) *via* a post-polymerization assembly strategy. The SPN systems were based on the copolymerization of naphthalimide pyridinium derivatives with acrylamide, followed by the electrostatic incorporation of exfoliated LP nanosheets, enabling hierarchical confinement regulation from hydrogels to freestanding films. The results demonstrated that the synergistic effect of hydrogen-bonding networks and rigid LP sheet architectures significantly suppressed non-radiative transitions of triplet excitons, extending the phosphorescence lifetime from initial 29.1 μs in the hydrogel state to 316.0 ms in dehydrated films with an extraordinary phosphorescence quantum yield of up to 67.5%. With these high-performance SPN systems, multifunctional dynamic information data processing and bioimaging of penetrating a piece of skin by employing the organic afterglow are successfully achieved. The proposed dual-confinement SPN fabricated by an eco-friendly and controllable method provides an alternative direction for designing high-efficiency supramolecular RTP materials.

Author contributions

This manuscript was written through contributions from all authors. All authors have given approval to the final version of the manuscript.

Conflicts of interest

There are no conflicts to declare.

Data availability

The data supporting this article have been included as part of the SI. Supplementary information: Compound synthesis and characterization and additional figures for the optical experiments. See DOI: **https://doi.org/10.1039/d5qm00579e**.

Acknowledgements

This work is supported by the National Natural Science Foundation of China (22301166), the Taishan Scholars Program (tsqn202408247), the Natural Science Foundation of Shandong Province (ZR2024MB132 and ZR2023QB186), the Innovative Research Programs of Higher Education of Shandong Province (2023KJ171), and the Open Research Project Fund of State Key Laboratory of Molecular Engineering of Polymers (K2025-10).

References

1 W.-L. Guan, J.-F. Chen, J. Liu, B. Shi, H. Yao, Y.-M. Zhang, T.-B. Wei and Q. Lin, Macrocycles-assembled AIE supramolecular polymer networks, *Coord. Chem. Rev.*, 2024, **507**, 215717.
2 L. Voorhaar and R. Hoogenboom, Supramolecular polymer networks: hydrogels and bulk materials, *Chem. Soc. Rev.*, 2016, **45**, 4013–4031.
3 D. Xia, P. Wang, X. Ji, N. M. Khashab, J. L. Sessler and F. Huang, Functional Supramolecular Polymeric Networks: The Marriage of Covalent Polymers and Macrocycle-Based Host–Guest Interactions, *Chem. Rev.*, 2020, **120**, 6070–6123.
4 J. Zhao, Z. Zhang, C. Wan and X. Yan, Synergistic Dual Dynamic Bonds in Covalent Adaptable Networks, *CCS Chem.*, 2024, **6**, 41–56.
5 F. Nie and D. Yan, Supramolecular Glass: A New Platform for Ultralong Phosphorescence, *Sci. China Mater.*, 2024, **67**, 3531–3536.
6 M. Ni, N. Zhang, W. Xia, X. Wu, C. Yao, X. Liu, X.-Y. Hu, C. Lin and L. Wang, Dramatically Promoted Swelling of a Hydrogel by Pillar[6]arene–Ferrocene Complexation with Multistimuli Responsiveness, *J. Am. Chem. Soc.*, 2016, **138**, 6643–6649.
7 X. Zhang, J. Zhuo, D. Wang and X. Zhu, Supramolecular Polymers for Drug Delivery, *Chem. Eur. J.*, 2025, **31**, e202404617.
8 J. Liu, Y.-Q. Fan, S.-S. Song, G.-F. Gong, J. Wang, X.-W. Guan, H. Yao, Y.-M. Zhang and T.-B. Wei, Aggregation-Induced

Emission Supramolecular Organic Framework (AIE SOF) Gels Constructed from Supramolecular Polymer Networks Based on Tripodal Pillar[5]arene for Fluorescence Detection and Efficient Removal of Various Analytes, *ACS Sustainable Chem. Eng.*, 2019, **7**, 11999–12007.

9 S. Jiang, X. Chen, P. Geng, H. Han, M. Xie and X. Liao, Supramolecular multicolor fluorescent hydrogels with a single fluorescent group based on host-guest Interactions, *Polym. Chem.*, 2025, **16**, 1537–1545.

10 X.-W. Sun, Z.-H. Wang, Y.-J. Li, Y.-F. Zhang, Y.-M. Zhang, H. Yao, T.-B. Wei and Q. Lin, Tri-pillar[5]arene-Based Multifunctional Stimuli-Responsive Supramolecular Polymer Network with Conductivity, Aggregation-Induced Emission, Thermochromism, Fluorescence Sensing, and Separation Properties, *Macromolecules*, 2021, **54**, 373–383.

11 L. Xu, Z. Wang, R. Wang, L. Wang, X. He, H. Jiang, H. Tang, D. Cao and B. Z. Tang, A Conjugated Polymeric Supramolecular Network with Aggregation-Induced Emission Enhancement: An Efficient Light-Harvesting System with an Ultrahigh Antenna Effect, *Angew. Chem., Int. Ed.*, 2020, **59**, 9908–9913.

12 Q. Duan, Q. Zhang, J. Zhang, S. Lin, T. Xiao and L. Wang, Artificial light-harvesting systems based on supramolecular polymers, *Chin. Chem. Lett.*, 2025, 111421.

13 L. Xu, R. Wang, H. Tang, L. Wang and D. Cao, An assembly-induced-emission orthogonal supramolecular network with spirobifluorene, pillararene, and tetraphenylethylene units for efficient light harvesting, *J. Mater. Chem. A*, 2022, **10**, 11332–11339.

14 Y. Cheng, X. Lv, B. Liang, X. Wei, P. Wang and D. Xia, Supramolecular polymer network gels constructed by a pillararene-containing polymer and their applications in adhesion between semihard materials, *Polym. Chem.*, 2023, **14**, 191–200.

15 G. Yao, M. Gao, Q. Zhang, X. Tan, C. Cai and S. Dong, Electric-Field Regulation of Adhesion/De-Adhesion/Release Capacity of Transparent and Electrochromic Adhesive, *Adv. Mater.*, 2025, **37**, 2500648.

16 H. Liu, S. Wei, H. Qiu, M. Si, G. Lin, Z. Lei, W. Lu, L. Zhou and T. Chen, Supramolecular Hydrogel with Orthogonally Responsive R/G/B Fluorophores Enables Multi-Color Switchable Biomimetic Soft Skins, *Adv. Funct. Mater.*, 2021, **32**, 2108830.

17 S. J. K. O'Neill, Z. Huang, M. H. Ahmed, A. J. Boys, S. Velasco-Bosom, J. Li, R. M. Owens, J. A. McCune, G. G. Malliaras and O. A. Scherman, Tissue-Mimetic Supramolecular Polymer Networks for Bioelectronics, *Adv. Mater.*, 2023, **35**, 2207634.

18 H.-Q. Peng, C.-L. Sun, L.-Y. Niu, Y.-Z. Chen, L.-Z. Wu, C.-H. Tung and Q.-Z. Yang, Supramolecular Polymeric Fluorescent Nanoparticles Based On Quadruple Hydrogen Bonds, *Adv. Funct. Mater.*, 2016, **26**, 5483–5489.

19 M. Du and C. Li, Engineering Supramolecular Hydrogels *via* Reversible Photoswitching of Cucurbit[8]uril-Spiropyran Complexation Stoichiometry, *Adv. Mater.*, 2024, **36**, 2408484.

20 M. Dai, Z. Qi and D. Yan, In Situ Generation of Microwire Heterojunctions with Flexible Optical Waveguide and Hydration-Mediated Photochromism, *Angew. Chem., Int. Ed.*, 2025, **64**, e202420139.

21 D. Dai, Z. Li, J. Yang, C. Wang, J.-R. Wu, Y. Wang, D. Zhang and Y.-W. Yang, Supramolecular Assembly-Induced Emission Enhancement for Efficient Mercury(II) Detection and Removal, *J. Am. Chem. Soc.*, 2019, **141**, 4756–4763.

22 Q. Lin, X.-W. Guan, Y.-M. Zhang, J. Wang, Y.-Q. Fan, H. Yao and T.-B. Wei, Spongy Materials Based on Supramolecular Polymer Networks for Detection and Separation of Broad-Spectrum Pollutants, *ACS Sustainable Chem. Eng.*, 2019, **7**, 14775–14784.

23 B. Hua, L. Shao, M. Li, H. Liang and F. Huang, Macrocycle-Based Solid-State Supramolecular Polymers, *Acc. Chem. Res.*, 2022, **55**, 1025–1034.

24 W. Zhang, J.-F. Chen, W.-J. Qu, Q. Lin, T.-B. Wei, H. Yao and B. Shi, Shape Memory Supramolecular Polymer Gels Constructed by Pillar[5]arene-Based Mechanically Interlocked Polymer Networks, *Macromolecules*, 2025, **58**, 178–186.

25 Y. Yang, S. Liu, H. Liu, Q. Li, H. Zhang, Z. Hu, X. Lu and X. Ji, Water-soluble fluorescent supramolecular polymer network with sustainable ''Fluorescence on'' based on AIEgen-containing host-guest interactions, *Giant*, 2022, **11**, 100112.

26 H. Li, Z. Huang, X. Huang, W. Huang, S. Rao, S. Liu, Y. Zhang and W. Tian, Host–Guest Interactions Induce Supramolecular Assembly and Inhibit Electron Transfer to Enhance the Fluorescence Emission of Supramolecular Polymers, *Macromolecules*, 2024, **57**, 1328–1336.

27 K. Lou, Z. Hu, H. Zhang, Q. Li and X. Ji, Information Storage Based on Stimuli-Responsive Fluorescent 3D Code Materials, *Adv. Funct. Mater.*, 2022, **32**, 2113274.

28 Y. Zhang, Y. Chen, H. Zhang, L. Chen, Q. Bo and Y. Liu, Slide-Ring Supramolecular Mechanoresponsive Elastomer with Reversible Luminescence Behavior, *Adv. Opt. Mater.*, 2023, **11**, 2202828.

29 X.-H. Wang, N. Song, W. Hou, C.-Y. Wang, Y. Wang, J. Tang and Y.-W. Yang, Efficient Aggregation-Induced Emission Manipulated by Polymer Host Materials, *Adv. Mater.*, 2019, **31**, 1903962.

30 M. Zhang, Y. Cheng, T. Zhang, B. Liang, X. Wei, P. Wang, D. Xia and X. Yan, A clusteroluminescent supramolecular polymer network constructed by pillararene and its application in information encryption, *Aggregate*, 2024, **5**, e608.

31 Q. Zhao, Y. Chen, S.-H. Li and Y. Liu, Tunable white-light emission by supramolecular self-sorting in highly swollen hydrogels, *Chem. Commun.*, 2018, **54**, 200–203.

32 Q. Zhou, C. Yang and Y. Zhao, Dynamic organic room-temperature phosphorescent systems, *Chem*, 2023, **9**, 2446–2480.

33 X.-Y. Dai, M. Huo and Y. Liu, Phosphorescence resonance energy transfer from purely organic supramolecular assembly, *Nat. Rev. Chem.*, 2023, **7**, 854–874.

34 Y. Yang, Q. Li and Z. Li, Advances in organic room-temperature phosphorescence: design strategies, photophysical mechanisms, and emerging applications, *Mater. Chem. Front.*, 2025, **9**, 744–753.

35 C. Xing, Z. Qi, Y.-J. Ma, D. Yan and W.-H. Fang, Dynamic Ultralong Phosphorescence and Optical Waveguiding Switches in Silver-Organic Complex *via* Reversible Single-Crystal-to-Single-Crystal Conversion, *Angew. Chem., Int. Ed.*, 2025, **64**, e202502782.
36 F. Nie and D. Yan, Bio-sourced flexible supramolecular glasses for dynamic and full-color phosphorescence, *Nat. Commun.*, 2024, **15**, 9491.
37 Y.-G. Wu, W.-L. Zhou, Y. Qiu, S. Wang, J. Liu, Y. Chen, X. Xu and Y. Liu, 4D Assembly of Time-dependent Lanthanide Supramolecular Multicolor Phosphorescence for Encryption and Visual Sensing, *Adv. Sci.*, 2025, **12**, 2415418.
38 L. Li, J. Zhou, J. Han, D. Liu, M. Qi, J. Xu, G. Yin and T. Chen, Finely manipulating room temperature phosphorescence by dynamic lanthanide coordination toward multilevel information security, *Nat. Commun.*, 2024, **15**, 3846.
39 Y. Li, Z. Huang, A. Shao, Z. Wu, Z. He, H. Tian and X. Ma, Aqueous up-conversion organic phosphorescence and tunable dual emission in a single-molecular emitter, *Chem. Sci.*, 2025, **16**, 6290–6297.
40 X. Zhou, X. Bai, F. Shang, H.-Y. Zhang, L.-H. Wang, X. Xu and Y. Liu, Supramolecular assembly activated single-molecule phosphorescence resonance energy transfer for near-infrared targeted cell imaging, *Nat. Commun.*, 2024, **15**, 4787.
41 J. Cheng, H. Sun, L. Zhou, G. V. Baryshnikov, M. Liu, S. Shen, H. Ågren and L. Zhu, Electrostatic interaction-mediated 1:1 complexes for high-contrast mitochondrial-targeted phosphorescence bioimaging, *Sci. China: Chem.*, 2024, **67**, 3406–3413.
42 C. Xing, B. Zhou, D. Yan and W.-H. Fang, Dynamic Photoresponsive Ultralong Phosphorescence from One-Dimensional Halide Microrods Toward Multilevel Information Storage, *CCS Chem.*, 2023, **5**, 2866–2876.
43 Q. Tian, Q. Ding, C. Xu, L. Qu, K. Wang, C. Yang and Y. Zhao, Dynamic Regulation of Radical Photochromism and Photoluminescence *via* Polymer Polarity, *Angew. Chem., Int. Ed.*, 2025, **64**, e202509506.
44 Z. He, J. Song, C. Li, Z. Huang, W. Liu and X. Ma, High-Performance Organic Ultralong Room Temperature Phosphorescence Based on Biomass Macrocycle, *Adv. Mater.*, 2025, **37**, 2418506.
45 Z. Wu, Z. Xu, D. Wang, G. Deng, S. Lin, Z. Zhao, D. Wang, Y. Xiong and B. Z. Tang, Positional Isomerism Toward Tunable Organic Afterglow and Reversible Photoactivation Behavior for Anti-Counterfeiting and Encryption, *Adv. Funct. Mater.*, 2025, **35**, 2415285.
46 M. Dai, B. Zhou and D. Yan, Rare Earth Single-Atomic Hybrid Glasses for Near-Infrared II Optical Waveguides, *Angew. Chem., Int. Ed.*, 2025, **64**, e202505322.
47 J.-Q. Zhao, D.-Y. Wang, T.-Y. Yan, Y.-F. Wu, Z.-L. Gong, Z.-W. Chen, C.-Y. Yue, D. Yan and X.-W. Lei, Synchronously Improved Multiple Afterglow and Phosphorescence Efficiencies in 0D Hybrid Zinc Halides With Ultrahigh Anti-Water Stabilities, *Angew. Chem., Int. Ed.*, 2024, **63**, e202412350.
48 J. Zhang, W. Wang, Y. Bian, Y. Wang, X. Lu, Z. Guo, C. Sun, Z. Li, X. Zhang, J. Yuan, Y. Tao, W. Huang and R. Chen, Exciton Dissociation and Recombination Afford Narrowband Organic Afterglow Through Efficient FRET, *Adv. Mater.*, 2024, **36**, 2404769.
49 F. Gu, M. Ji, L. Zhang, T. Zhao, R. Zhang, X. Lv, H. Tian and X. Ma, Visualization of photocuring and 4D printing with real-time phosphorescence, *Nat. Commun.*, 2025, **16**, 4173.
50 X. Dou, X. Wang, X. Xie, J. Zhang, Y. Li and B. Tang, Advances in Polymer-Based Organic Room-Temperature Phosphorescence Materials, *Adv. Funct. Mater.*, 2024, **34**, 2314069.
51 J. Guo, C. Yang and Y. Zhao, Long-Lived Organic Room-Temperature Phosphorescence from Amorphous Polymer Systems, *Acc. Chem. Res.*, 2022, **55**, 1160–1170.
52 Q. Song, Z. Liu, X. Bai, Y. Zhang, S. Yang, Y. Ge and X.-Y. Dai, Achieving Robust Phosphorescence Supramolecular Polymeric Hydrogels by Green In Situ Iodoisoquinolinium Binary Copolymerization, *Adv. Opt. Mater.*, 2025, **13**, 2500624.
53 J. Huang, L. Qu, L. Gao, X. Wang, Q. Chen, Y. Wang, Y. Zhu, C. Li, Y. Li and C. Yang, Multicolor Room-Temperature Phosphorescence Achieved by Intrinsic Polymers Containing Solely One Phosphor Unit, *Macromolecules*, 2024, **57**, 4321–4330.
54 H. Chen, Y. Zhang, J. Shan, M. Dong, Z. Qian, A. Lv, H.-J. Qian, H. Ma, Z. An, L. Gu and W. Huang, Water-Resistant Organic Room-Temperature Phosphorescence from Block Copolymers, *Angew. Chem., Int. Ed.*, 2025, **64**, e202500610.
55 N. Gan, X. Zou, Z. Qian, A. Lv, L. Wang, H. Ma, H.-J. Qian, L. Gu, Z. An and W. Huang, Stretchable phosphorescent polymers by multiphase engineering, *Nat. Commun.*, 2024, **15**, 4113.
56 B. Ding, X. Ma and H. Tian, Recent Advances of Pure Organic Room Temperature Phosphorescence Based on Functional Polymers, *Acc. Mater. Res.*, 2023, **4**, 827–838.
57 P. Chen, H. Qie, X. Yang, S. Ma, Z. Wang, N. Li, Y. Deng, F. Bian and S. Lü, Luminous Fish-Inspired Hydrogels with Underwater Long-Lived Room Temperature Phosphorescence, *Adv. Funct. Mater.*, 2025, **35**, 2416430.
58 H. Su, K. Hu, W. Huang, T. Wang, X. Zhang, B. Chen, H. Miao, X. Zhang and G. Zhang, Functional Roles of Polymers in Room-Temperature Phosphorescent Materials: Modulation of Intersystem Crossing, Air Sensitivity and Biological Activity, *Angew. Chem., Int. Ed.*, 2023, **62**, e202218712.
59 T. Zhang, X. Ma and H. Tian, A facile way to obtain near-infrared room-temperature phosphorescent soft materials based on Bodipy dyes, *Chem. Sci.*, 2020, **11**, 482–487.
60 F. Guo, Y. Chen, C. Li, X. Wang, Q. Li, M. He, H. Hou and C. Yang, Visualization Detection of Ultralow Temperature Based on Flexible Cross-linked Polymer Systems, *Adv. Funct. Mater.*, 2025, **35**, 2416465.
61 S. Kuila, K. V. Rao, S. Garain, P. K. Samanta, S. Das, S. K. Pati, M. Eswaramoorthy and S. J. George, Aqueous Phase Phosphorescence: Ambient Triplet Harvesting of

Purely Organic Phosphors *via* Supramolecular Scaffolding, *Angew. Chem., Int. Ed.*, 2018, **57**, 17115–17119.

62 X. Chen, C. Xu, T. Wang, C. Zhou, J. Du, Z. Wang, H. Xu, T. Xie, G. Bi, J. Jiang and X. Zhang, Versatile Room-Temperature-Phosphorescent Materials Prepared from N-Substituted Naphthalimides: Emission Enhancement and Chemical Conjugation, *Angew. Chem., Int. Ed.*, 2016, **55**, 9872–9876.

63 Z. Huang, Z. He, B. Ding, H. Tian and X. Ma, Photoprogrammable circularly polarized phosphorescence switching of chiral helical polyacetylene thin films, *Nat. Commun.*, 2022, **13**, 7841.

